11–12 (2021) 100067

Contents lists available at ScienceDirect

Journal of Non-Crystalline Solids: X

journal homepage: www.sciencedirect.com/journal/journal-of-non-crystalline-solids-x

Liquid–liquid phase transition in simulations of ultrafast heating and decompression of amorphous ice

Nicolas Giovambattista [a,b,*], Peter H. Poole [c,*]

[a] Department of Physics, Brooklyn College of the City University of New York, Brooklyn, NY 11210, United States
[b] Ph.D. Programs in Chemistry and Physics, The Graduate Center of the City University of New York, New York, NY 10016, United States
[c] Department of Physics, St. Francis Xavier University, Antigonish, NS B2G 2W5, Canada

ARTICLE INFO

Keywords:
Supercooled water
Amorphous ice
Phase transition
Computer simulation

ABSTRACT

A recent experiment [K. H. Kim, *et al.*, Science **370**, 978 (2020)] showed that it may be possible to detect a liquid–liquid phase transition (LLPT) in supercooled water by subjecting high density amorphous ice (HDA) to ultrafast heating, after which the sample reportedly undergoes spontaneous decompression from a high density liquid (HDL) to a low density liquid (LDL) via a first-order phase transition. Here we conduct computer simulations of the ST2 water model, in which a LLPT is known to occur. We subject various HDA samples of this model to a heating and decompression protocol that follows a thermodynamic pathway similar to that of the recent experiments. Our results show that a signature of the underlying equilibrium LLPT can be observed in a strongly out-of-equilibrium process that follows this pathway despite the very high heating and decompression rates employed here. Our results are also consistent with the phase diagram of glassy ST2 water reported in previous studies.

1. Introduction

Starting in the 1970s, interest in the properties of water and amorphous ice expanded greatly in response to the seminal discoveries made by Austen Angell and coworkers on the anomalous properties of supercooled water [1,2]. Although the proposal of a liquid–liquid phase transition (LLPT) in supercooled water to explain these anomalies was first presented almost three decades ago [3], experiments seeking to confirm and locate the LLPT remain challenging [4–10]. The LLPT separates two distinct phases of liquid water, low-density liquid (LDL) and high-density liquid (HDL), which are proposed to be the liquid-state manifestations of the two experimentally known forms of amorphous ice, low-density amorphous (LDA) and high-density amorphous (HDA) ice (see, e.g. Refs. [11–18]). The estimated location of the LLPT in the phase diagram of water places it at deeply supercooled temperatures for the liquid phase and at elevated pressures in the kbar range [11,19–22]. Under these conditions, the supercooled liquid rapidly transforms to the stable ice phase, and so an experiment to detect the LLPT must measure properties of the metastable liquid state on a time scale long enough to capture the behavior of the liquid in equilibrium, but do so fast enough to complete the measurement before ice nucleation eliminates the liquid phase [23].

A recent experimental study [24] addressed these challenges using a novel method to prepare HDL under pressure via ultrafast (&100 fs) isochoric heating of HDA using an IR laser pulse. The HDL sample so created then relaxed (i.e. decompressed) to ambient pressure on a sub-μs time scale, triggering the phase transition to LDL, followed by crystallization on a longer time scale of approximately 10 μs. Short (<50 fs) X-ray laser pulses were used to measure the time evolution of the structure factor during the decompression of the HDL sample to ambient pressure, and revealed the conversion of the sample to LDL prior to crystallization. Ref. [24] also presented simulation results to support the interpretation of the experimental data. Using the ST2 model of water, in which the occurrence of a LLPT is well documented [3,25–27], Ref. [24] provided simulation evidence that the HDL state can be accessed by ultrafast isochoric heating of HDA, and that the subsequent decompression of HDL exhibits a sudden density decrease associated with the LLPT.

In the present work, we use computer simulations to study the same kind of thermodynamic pathway explored in Ref. [24], but over a much broader range of conditions, in order to clarify the response of the system when subjected to such rapid changes of state. Here we also use the ST2 model, which provides a system in which we know that the equilibrium liquid exhibits a LLPT. The simulation results presented in

* Corresponding authors.
E-mail addresses: ngiovambattista@brooklyn.cuny.edu (N. Giovambattista), ppoole@stfx.ca (P.H. Poole).

https://doi.org/10.1016/j.nocx.2021.100067
Received 22 June 2021; Received in revised form 1 September 2021; Accepted 2 September 2021
Available online 14 September 2021
2590-1591/© 2021 The Authors. Published by Elsevier B.V. This is an open access article under the CC BY-NC-ND license (http://creativecommons.org/licenses/by-nc-nd/4.0/).

Ref. [24] studied an HDA sample at a single density (1.30 g/cm^3) and heated to three temperatures (200, 230 and 250 K), at which the decompression step was explored. Here we present results for HDA samples prepared at four different densities, and at different heating rates. We also explore the decompression process over a wide range of temperatures, spanning both glassy and equilibrium liquid states. In addition, we examine the effect of changing the rate of decompression. We also compare the thermodynamic pathways explored in our simulations to the crystallization and glass transition boundaries known for ST2 water from previous work. As we will see, this comparison allows us to clarify how the LLPT manifests itself when following different pathways in the water phase diagram. Our results thus provide additional support for the interpretation that the experiments of Ref. [24] probe the LLPT in water.

Our simulation results confirm that rapid isochoric heating of ambient-pressure HDA is able to drive the sample into the HDL region of the phase diagram at pressures above the coexistence line of the LLPT. Our simulations also reproduce the signature of the LLPT during the relaxation of the sample back to ambient pressure. We find that even when equilibrium liquid states of HDL and LDL do not have time to be established during this process, the signature of the underlying HDL-LDL transition can be observed in the response of the system. Overall, our simulations confirm the interpretation of the thermodynamic pathway explored in Ref. [24] and demonstrate that ultrafast manipulation of samples of amorphous ice and supercooled water can be used to confirm the existence, and also find the location, of the LLPT in the phase diagram of water.

2. Experimental pathway

In the experiments of Ref. [24], HDA samples are produced under pressure and then recovered under vacuum (pressure $P \approx 0$) at temperatures T in the range $T = 78$ to 115 K. These HDA samples are then subjected to a process of rapid heating followed by density relaxation along the thermodynamic path depicted in Fig. 1.

The details of this procedure are as follows. Prior to the heating process, the HDA samples are at an initial pressure of $P_i \approx 0$ and initial temperature $T_i = 115$ K. Under these conditions, Ref. [24] estimates that the initial density ρ_i of the HDA sample is in the range 1.13 to 1.16 g/cm^3. The HDA sample is then rapidly heated from T_i to a final temperature $T_f = 205 \pm 10$ K using an infrared (IR) laser pulse that lasts for approximately 100 fs. The corresponding heating rate was estimated to be $q_T \simeq 4500$ K/ns [24]. As explained in Ref. [24], this heating process occurs much faster than the rate, governed by the speed of sound in the sample, required for the sample density to respond to the change in T. As a result, the volume of the sample remains approximately constant and so the heating process is isochoric.

Since the heating process is isochoric, immediately after the IR pulse is applied, the sample density is still ρ_i but the sample temperature is now $T_f \approx 205$ K. Based on experimental data for supercooled liquid water, Ref. [24] shows that a liquid sample at this density and temperature would be found at $P = 300 \pm 50$ MPa and have a liquid-state relaxation time of less than 10 ns. Therefore, within a few ns of the IR heating process, the sample is in the equilibrium HDL state at $T \approx 205$ K and $P \approx 300$ MPa. However, the surface of the sample is exposed to ambient pressure conditions ($P \approx 0$), and so the sample density immediately begins to decrease as the system relaxes toward the lower equilibrium density expected at $P \approx 0$. In Ref. [24] this density relaxation is described as a "decompression" process because the pressure inside the sample is decreasing from a high value, transiently imposed by the IR pulse, to $P \approx 0$. The sample temperature remains constant during the density relaxation for approximately 100 μs, until heat conduction from the surroundings begins to cool the sample. That is, during the first 100 μs, the density relaxation process is analogous to an isothermal decompression.

During this isothermal decompression, the structure of the sample is studied using short (<50 fs) X-ray pulses over a time window of 8.4 ns to 1 ms after the IR pulse is applied. From the evolution of the structure factor with time, Ref. [24] shows that the sample converts from HDL to LDL during the isothermal decompression, before crystallization intervenes on a time scale of approximately 10 μs. Since the pressure inside the sample is not measured in these experiments, it is not clear what the decompression rate q_P is. However, it is estimated that the HDL-to-LDL transformation occurs within 10–100 ns after the IR pulse [24]. In the Supplementary Material of Ref. [24] it is estimated that the decompression process lasts for 70 ns, giving an experimental decompression rate of approximately $q_P = 4.3$ MPa/ns.

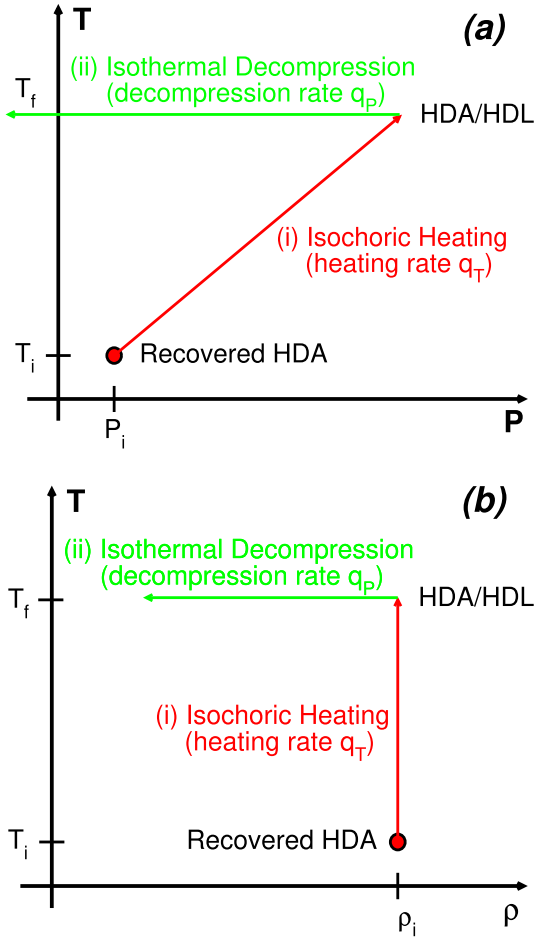

Fig. 1. Schematic diagrams showing the paths in the (a) T-P and (b) T-ρ planes followed during our computer simulations, which mimic the experiments of Ref. [24]. An HDA sample is recovered at pressure P_i and temperature T_i with density ρ_i. The recovered HDA sample is then heated at constant density at rate q_T up to a temperature T_f. Depending on the value of T_f, the sample may be found in the HDA or HDL state. The HDL/HDA so produced is then decompressed at constant temperature T_f. In our computer simulations, $T_i = 80$ K and various values of T_f and P_i are explored ($T_f = 100$ to 300 K, $P_i = -100$ to 1150 MPa). In the experiments of Ref. [24], $T_i = 115$ K, $T_f \approx 205$ K, and $P_i \approx 0$ MPa. (For interpretation of the references to color in the text, the reader is referred to the web version of this article.)

3. Simulation methods

In this work, we conduct out-of-equilibrium molecular dynamics simulations of a system composed of $N = 1728$ water molecules in a cubic box with periodic boundary conditions. We employ the ST2 water model [29], which exhibits a LLPT and associated liquid–liquid critical point (LLCP) in the supercooled liquid domain. The critical values of the

temperature, pressure and density for the LLCP in ST2 are respectively $T_c = 247 \pm 3$ K, $P_c = 185 \pm 15$ MPa, and $\rho_c = 0.955 \pm 0.01$ g/cm^3 [3,23,25,27,30,31]. The ST2 water model has been used extensively to study the behavior of water in the liquid [3,23,26,27] and glassy states [32–38]. For consistency with previous studies, we treat the long-range electrostatic interactions using the reaction field technique [39]. Refs. [28,34,35] provide reference data sets for the ST2 system employed here. In all simulations, T and P are controlled using a Berendsen thermostat and barostat, respectively. The time constant τ_T used for the thermostat is 0.5 ps. The barostat depends on the ratio τ_P/κ, where κ is the isothermal compressibility and τ_P is the barostat relaxation time. In this work, we use $\tau_P/\kappa = 50$. For typical values of κ for ST2 water, this choice corresponds to values of τ_P in the range 0.05 ± 0.03 ps.

To carry out cooling or heating runs, we change the thermostat temperature linearly with time at a rate q_T. To conduct compression or decompression runs, the barostat pressure changes linearly at a rate q_P; see Ref. [34] for details. For each cooling, heating, compression, or decompression study, we generate 10 independent starting configurations using the same protocol for sample preparation. These 10 configurations are then subjected to the chosen process, allowing us to assess the magnitude of the sample-to-sample variation due to differences in the starting configurations.

Our starting samples of HDA are created via the procedure described in detail in Refs. [34–38] and illustrated schematically in Fig. 2(a). We first produce LDA by cooling the equilibrium liquid from $T = 350$ K to $T = 80$ K at constant $P = 0.1$ MPa using a cooling rate $q_T = 30$ K/ns. This LDA sample is then compressed isothermally at $T = 80$ K from $P = 0.1$ MPa to $P = 1700$ MPa using a compression rate $q_P = 300$ MPa/ns. Fig. 2b shows the density of 10 independent simulations during the compression of LDA. The sharp change in density at $P \approx 1100$ MPa indicates the transformation of LDA to HDA. The HDA samples produced by this transformation are then decompressed at the same $T = 80$ K and rate q_P used during the compression of LDA. The density of HDA during the decompression process is shown in Fig. 2b. In this work, HDA samples produced by decompressing HDA to pressures below $P = 1100$ MPa are denoted as HDA-d. The sharp density change at $P \approx -400$ MPa indicates the conversion of HDA back to LDA [34,36].

The sudden decrease in density observed at $P \approx -550$ MPa in Fig. 2b corresponds to the limit of mechanical stability of our LDA samples at which they fracture under hydrostatic tension. Beyond this limit, empty voids appear in the system separating isolated groups of molecules. The analogous mechanical stability limit of the liquid state corresponds to cavitation, the formation of vapor bubbles in the liquid phase when under tension.

For the present simulations, we seek to study heating-decompression processes similar to that realized in the experiments of Ref. [24] and described in Section 2. This pathway starts with a sample of HDA at an initial temperature T_i and initial pressure P_i, corresponding to an initial density ρ_i, as depicted in Fig. 1. This sample is heated isochorically to a final temperature T_f, followed by an isothermal decompression carried out at T_f. In the experiments, $T_i = 115$ K and $P_i \approx 0$, and $T_f \approx 205$ K.

In our simulations, we chose $T_i = 80$ K, the temperature at which the compression/decompression cycle to produce the samples of HDA-d have been conducted in this and in several previous studies of ST2. We note that the density of HDA samples recovered at ambient pressure varies [40]. In order to test if variations in ρ_i influence the results of the heating-decompression process studied here, we recover starting samples of HDA-d at $T_i = 80$ K at a set of four different initial densities $\rho_i \in \{1.30, 1.36, 1.43, 1.48\}$ g/cm^3. Due to the variations that occur across the 10 independent decompression runs used to produce the recovered HDA-d samples, the pressures for the samples at each density varies over a finite interval. The intervals of P_i corresponding to the set of values of ρ_i are $P_i \in \{(-200, -100), (-25, 100), (375, 550), (900, 1150)\}$ MPa. The range of samples so produced allows us to test if varying the density of the starting HDA-d sample affects the conditions at which HDA/HDL transforms to LDA/LDL during the decompression

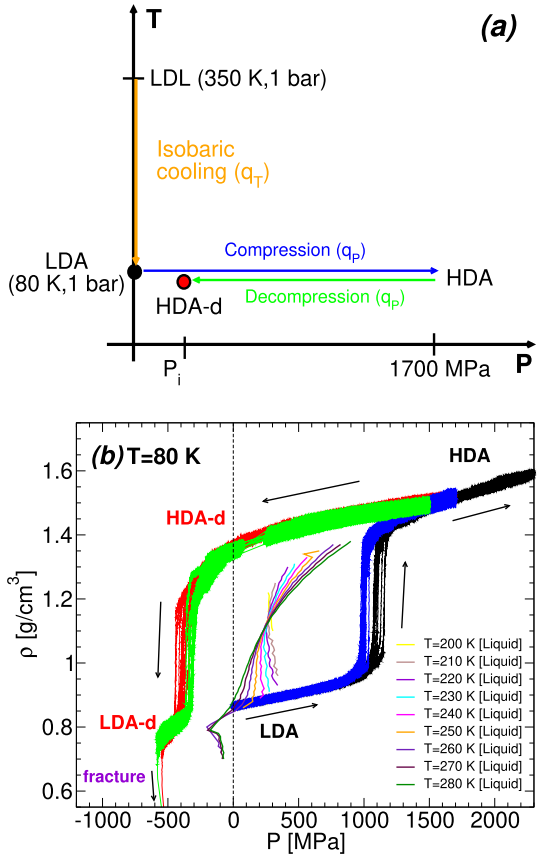

Fig. 2. (a) Schematic diagram showing the process followed in our simulations to prepare HDA-d. (b) Density as function of pressure during the pressure-induced LDA-to-HDA transformation and subsequent HDA-to-LDA transformation at $T = 80$ K [right-arrows and left-arrows in (a)]. Black and red lines are obtained with a compression/decompression rate $q_P = 300$ MPa/ns; blue and green lines correspond to $q_P = 30$ K/ns. All 10 independent runs are included. The sharp density changes at $P \approx 1000$ and 1100 MPa indicate the compression-induced LDA-to-HDA transformation. The sudden changes in density at $P \approx -350$ and -400 MPa signal the decompression-induced HDA-to-LDA transformations. Recovered LDA samples fracture at $P \approx -550$ MPa. For comparison, we also include the isotherms of the equilibrium liquid at temperatures below and above the LLCP temperature $T_c \approx 245$ K ($\rho_c \approx 0.955$ g/cm^3) from Ref. [28]. Reducing the compression/decompression rate q_P reduces the hysteresis during the LDA-HDA transformation, bringing the LDA-to-HDA transformation paths (black and blue lines) as well as the HDA-to-LDA transformation paths (red and green lines) closer to the low-temperature liquid isotherms. "Fracture" labels the limit of mechanical stability of the amorphous solid under tension. (For interpretation of the references to color in this figure legend, the reader is referred to the web version of this article.)

step of the heating-decompression process.

In addition, in order to provide a more general understanding of the thermodynamic pathway utilized in the experiments of Ref. [24], we explore the effect of varying T_f, the temperature at the end of the heating stage and at which the isothermal decompression stage is carried out. We vary T_f over the range 100 to 300 K, which encompasses the glassy state (approximately $T < 210$ K) and the liquid state (approximately $T > 210$ K), both below and above the temperature of the LLCP for ST2.

For the isochoric heating stage of the heating-decompression process, the heating rate employed in our simulations is $q_T = 30$ K/ns. This is approximately 100 times slower than the experimental heating rate. While we could conduct simulations at the experimental rate, using $q_T = 30$ K/ns allows us to compare our results to those obtained in previous ST2 simulation studies of amorphous ice that used the same rate. This rate also allows our samples to pass through the glass

transition temperature T_g for the simulated system and access the equilibrium liquid state (when $T_f > T_g$) during the heating process itself. Thus by tuning T_f, we are choosing whether the decompression stage starts with a glass (HDA) or a liquid (HDL).

For the isothermal decompression stage that follows the heating stage, the decompression rate in our simulations is $q_P = 300$ MPa/ns. This decompression rate is approximately 100 times faster than the rate estimated in the experiments [24]. A subset of our runs have been reproduced using a slower rate of $q_P = 30$ MPa/ns. These results are presented in Sec. I of the Supplementary Material (SM) and do not qualitatively change our conclusions. On this basis, we do not expect that a further reduction of the rate to the experimental value of $q_T = 4.3$ MPa/ns will markedly affect our results.

4. Results

4.1. Isochoric heating

The schematic diagram shown in Fig. 1 assumes that during the isochoric heating process, the pressure of HDA increases with increasing temperature (red arrow). However, the experiments of Ref. [24] do not provide the pressure of the system upon heating or decompression. We show in Fig. 3 the pressure as directly measured in our simulations during the isochoric heating of HDA-d samples with different values of ρ_i, which therefore begin the heating process at different values of P_i. We find that for our smallest value of $\rho_i = 1.30$ g/cm^3, corresponding to samples with the lowest P_i, the pressure of the HDA-d samples indeed increases upon heating, confirming the assumption of Fig. 1 and Ref. [24]. However, the variation of P with T is not linear, or even monotonic, up to $T_f \approx 220$ K at the heating rate used here. For larger ρ_i, P initially increases with T, and then reaches a maximum and decreases with T as $T_f \to 220$ K. We show in the SM (Sec. II) that at the much faster heating rate of $q_T = 3000$ K/ns, which is closer to the experimental rate, the variation of P with T for $\rho_i = 1.30$ g/cm^3 approaches a linear relation [24]. This result is consistent with the expectation that in the limit of infinitely fast heating, the increase in P with T will be dominated by the ideal gas contribution to P, which is linear in T at fixed density.

To place these results in context, we also show in Fig. 3 three boundaries obtained in earlier work characterizing the behavior of the ST2 system. (i) We show the boundary in the P-T plane where crystallization to the high-pressure ice VII phase was observed in Ref. [34] during isothermal compression of ST2 water ($q_P = 300$ MPa). This crystallization region occurs inside the nose-shaped area indicated by the black solid line at $P > 700$ MPa and centered at $T \approx 250$ K. (ii) The orange up-triangles at $T = 250$ K indicate the temperature at which HDA/HDL crystallizes during isobaric heating (with $q_T = 30$ K/ns) for $P > 400$ MPa. (iii) We also show the boundary in the P-T plane at which the HDA-to-LDA and HDA-to-HDL transformations occur upon isobaric heating, as reported in Ref. [35]. As shown in Refs. [33,35], these HDA-to-LDA and HDA-to-HDL transformations define a single line in the P-T plane that represents the limit of stability of HDA relative to LDA or HDL during isobaric heating. This metastability limit is indicated approximately by the maroon dashed line in Fig. 3 (for the case $q_T = 30$ K/ns). We note that the HDA-to-LDA transformation line in the P-T plane, when measured using ultrafast rates, is sensitive to the procedure followed. For example, in Fig. 3 the HDA-to-LDA transformation induced by isobaric heating with $q_T = 30$ K/ns at low and negative pressures (dashed maroon line) differs from the HDA-to-LDA transformation induced by isothermal decompression with $q_P = 300$ MPa/ns (orange left-triangles). As expected, these differences in the locations of the HDA-to-LDA transformation lines in the P-T plane decrease as the rates employed (q_T or q_P) decrease [34,35].

We observe crystallization during our isochoric heating runs at all densities ρ_i. As shown in Sec. III of the SM, crystallization is readily detected by monitoring the oxygen–oxygen radial distribution function of the system upon heating, and occurs in the range $T = 230$–260 K. At $\rho_i = 1.30$ g/cm^3, 2 out of the 10 independent runs crystallize. At $\rho_i = 1.36$ g/cm^3, 9 out of the 10 independent runs crystallize. For all larger values of ρ_i, all runs crystallize. In Fig. 3, we plot the pressure for each heating run only up to the temperature where crystallization occurs. The crystallization behavior observed here is largely consistent with the boundaries for the onset of crystallization found in previous work during isothermal compression (solid black line) and isobaric heating (orange up-triangles). The exceptional case occurs for $\rho_i = 1.30$ g/cm^3, where 8 out of 10 runs resist crystallization, allowing the system to be heated well into the liquid phase up to 350 K. The

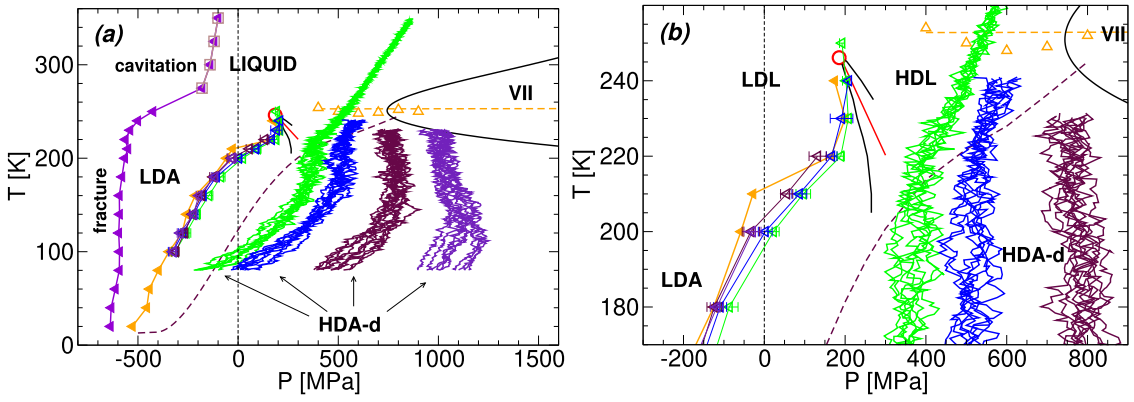

Fig. 3. (a) Temperature as function of pressure upon heating HDA-d at $\rho_i = 1.30$ (green lines), $\rho_i = 1.36$ (blue lines), $\rho_i = 1.43$ (maroon lines), and $\rho_i = 1.48$ g/cm^3 (indigo lines). The starting HDA-d configurations are obtained by decompressing HDA at $T = 80$ K from $P = 1700$ MPa until the system reaches the target density ρ_i; see red lines in Fig. 2 for the case $q_P = 300$ MPa/ns. Heating trajectories are shown only for temperatures at which crystallization is absent. Empty left-triangles represent the HDA-to-LDA transformation obtained upon isothermal decompression of the HDA-d samples heated at ρ_i; see Fig. 4. For comparison, also included are the HDA-to-liquid (at high pressure) and HDA-to-LDA (at low and negative pressure) transformations upon isobaric heating (maroon dashed-line) from Ref. [35]. Crystallization to ice VII occurs upon isothermal compression at $P > 700$ MPa and $T = 210$–300 K (solid black line) [34], and during isobaric heating of HDA at $T \approx 250$ K and $P > 400$ MPa (orange up-triangles and dashed line) [35]. Solid orange and indigo left-triangles represent, respectively, the HDA/HDL-to-LDA/LDL and LDA/LDL-to-vapor transformations during isothermal decompression of HDA samples with no heating treatment, reported in Ref. [34]. Squares locate the equilibrium liquid-to-vapor spinodal line, as estimated in Ref. [28]. "Fracture" labels the limit of mechanical stability of the amorphous solid under tension. "Cavitation" labels the limit of mechanical stability of the liquid phase under tension. (b) Magnification of panel (a). All compressions/decompressions are performed at rate $q_P = 300$ MPa/ns; all isochoric/isobaric heatings are performed at the rate $q_T = 30$ K/ns. (For interpretation of the references to color in this figure legend, the reader is referred to the web version of this article.)

absence of crystallization in an isochoric run which passes through a state point at which an isobaric run would reliably crystallize is likely a finite-size effect in our simulations.

We also find that all our runs at $\rho_i = 1.30$ and 1.36 g/cm^3 crossover from the glassy HDA state to the liquid HDL state in the range $T = 210$ to 220 K, regardless of whether the runs crystallize at higher T. This crossover corresponds to the glass transition temperature T_g encountered when heating the ST2 system at these densities at $q_T = 30$ K/ns. As shown in SM Sec. III, at T_g the mean-square displacement of the molecules becomes non-negligible, and the temperature dependence of the pressure and total energy shows the characteristic change in slope consistent with passing through the glass transition. Similarly, in Fig. 3, we see that the variation of P with T at $\rho_i = 1.30$ g/cm^3 changes behavior and becomes linear for $T > 210$ K, for those runs that do not crystallize. This behavior is consistent with the T_g boundary (maroon dashed line) found in previous work from isobaric heating runs at the same $q_T = 30$ K/ns. That is, our runs at $\rho_i = 1.30$ and 1.36 g/cm^3 enter a window of T between T_g and the crystallization temperature within which the HDL phase is accessed in our simulations. As shown in Fig. 3, our runs at $\rho_i = 1.43$ and 1.48 g/cm^3 crystallize before they reach T_g, and so the HDL phase is not observed in these runs prior to crystallization.

Based on the above observations, our simulations thus confirm that rapid isochoric heating provides a method to drive a sample of HDA at low-T and ambient-P to a location in the phase diagram corresponding to the equilibrium HDL phase at pressures above the coexistence line of the LLPT, just as proposed in the experiments of Ref. [24].

4.2. Isothermal decompression

We next carry out isothermal decompression at fixed $T = T_f$ of HDA-d samples heated at constant ρ_i to various temperatures T_f in the range from 100 to 300 K. Fig. 4(a) shows ρ for each sample as function of P during these isothermal decompression runs for different T. All these samples have an initial density, prior to decompression, of $\rho_i = 1.30$ g/cm^3 and, depending on T, they correspond to HDA (for $T_f \lessapprox 210$ K) or HDL (for $T_f \gtrapprox 210$ K). As shown in Fig. 4(a), all samples exhibit a density change during decompression characteristic of the transformation to an LDA or LDL-like state. The sharpness of the density change depends on T. In particular, for $T < 200$ K where the system is a glass at all P, the HDA-to-LDA transformations are reminiscent of a sharp, discontinuous first-order phase transition. Similar abrupt density changes occur during the pressure-induced LDA-HDA transformation cycles at $T = 80$ K [34] (red and black lines). At $T > 200$ K, the high-density to low-density

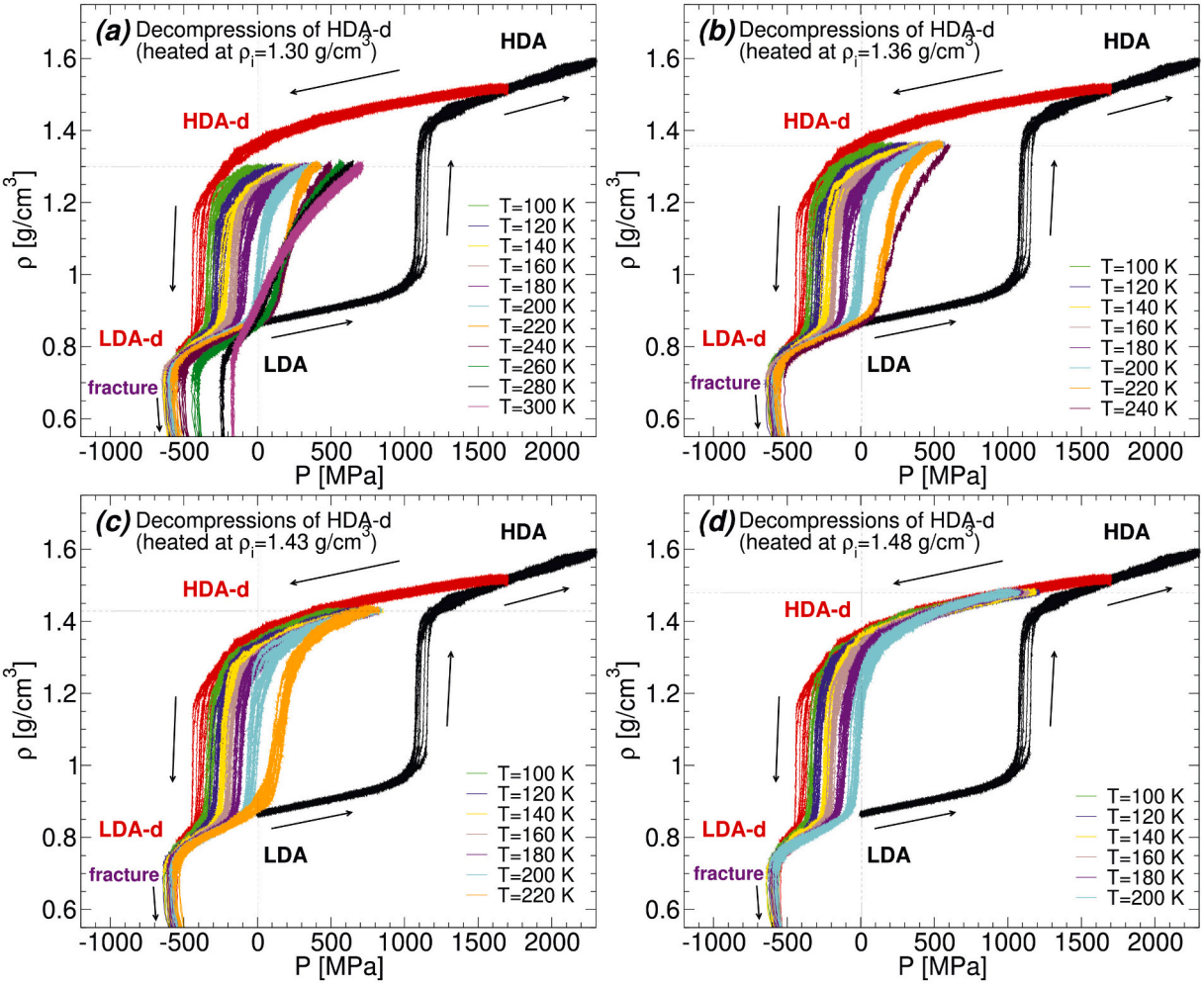

Fig. 4. Density as function of pressure during the isothermal decompression of HDA-d samples at different temperatures T. The HDA-d samples are prepared by isochoric heating at density ρ_i, from $T = 80$ K to the target temperature T. (a) $\rho_i = 1.30$ g/cm^3, (b) $\rho_i = 1.36$ g/cm^3, (c) $\rho_i = 1.43$ g/cm^3, and (d) $\rho_i = 1.30$ g/cm^3. Also included are the pressure-induced LDA-to-HDA and HDA-to-LDA transformations at $T = 80$ K from Fig. 2 (black and red lines). All compression/decompressions are performed at $q_P = 300$ MPa/ns. Some HDA-d samples crystallize during decompression at approx $T > 230$ K and are not included for clarity. "Fracture" labels the limit of mechanical stability of the system under tension. (For interpretation of the references to color in this figure legend, the reader is referred to the web version of this article.)

transformation as a function of P becomes smoother but still follows a curve where ρ has a well-defined inflection point. At the highest $T > 280$ K this inflection point is weak or absent, consistent with entering the T-range well above the LLCP where such an inflection would also be weak or absent in the equilibrium system; see Fig. 1. The pattern of behavior shown in Fig. 4(a) is observed for all values of ρ_i studied here, as shown in Fig. 4(b)–(d), demonstrating that the occurrence of the high-density to low-density transformation is insensitive to the density at which HDA or HDL is prepared.

In Sec. IV of the SM, we test if changing the preparation pathway for our starting HDA samples influences our results. Specifically, we prepare HDA samples by instantaneous isochoric quenches to $T = 80$ K, starting from the equilibrium liquid state at $P = 400$ MPa and $T = 220$ or 300 K. After adjusting the density of these quenched samples to match $\rho_i = 1.30$ g/cm^3, they are subjected to the same two-stage process of isochoric heating and isothermal decompression applied to our HDA-d samples. We find that the high-density to low-density transformation is again observed, demonstrating that our results are independent of the method followed to prepare the starting HDA sample of the heating runs.

Notably, the pressure of the high-density to low-density transformation at fixed T is independent of the density ρ_i at which HDA-d is prepared. This is shown in Fig. 3, where the pressure of this transformation $P_{H\to L}$ is presented as a function of T for each of the values of ρ_i studied here. We define $P_{H\to L}$ as the pressure, averaged over the 10 independent runs, at which the sample density passes through $\rho = 1.05$ g/cm^3. As shown in Fig. 4(a)–(d), this density corresponds approximately to the midpoint of the high-density to low-density transition. Also shown in Fig. 3, all values of $P_{H\to L}$ coincide with the $P_{H\to L}$ values obtained in Ref. [34] via decompression of HDA samples prepared by compression of LDA at fixed T. This demonstrates that the behavior observed during decompression is robustly insensitive to the method by which HDA samples under pressure are prepared, whether it be by ultrafast isochoric heating (as studied here and in Ref. [24]) or by isothermal compression [34].

To monitor the structural change in the system during decompression, we show in Fig. 5 the structure factor $S(q)$ for O atoms as a function of wave number q, for various pressures during the isothermal decompression carried out at $T = 200$ K, starting from our HDA-d samples having density 1.30 g/cm^3. This decompression path is shown as the cyan curve in Fig. 4(a), and starts from HDA-d samples that have been heated to the vicinity of the T_g value where they become HDL; see Fig. 3. In Fig. 5, each curve is evaluated by averaging over the set of configurations (typically 20) from all 10 independent decompression runs that occur within ±10 MPa of the indicated pressure. The qualitative pattern of change in $S(q)$ with pressure is the same as that observed in the experimental $S(q)$ data presented in Ref. [24]. There are distinct line shapes characteristic of HDA or LDA, and as P changes, the HDA line shape is most prominent at high P, while the LDA line shape is most prominent at low P. Similar to the experimental $S(q)$, this change does not occur via a continuation change in the q-value of a particular peak. Rather, one set of features, with approximately fixed q, is exchanged for another, indicating that one type of local structure is being replaced by a distinct local structure during decompression. We also note that the value of $S(q)$ as $q \to 0$ is largest at intermediate P corresponding to the pressure where the most rapid density change occurs in Fig. 4(a). This behavior is consistent with the presence of large scale spatial fluctuations of density occurring during the transition, and suggests the existence of distinct HDA and LDA domains. This behavior is also consistent with discontinuous structural change in the sample during decompression. We also note that while $S(q)$ for LDA is consistent with experiments, differences in the $S(q)$ for HDA from ST2 water and experiments are observed, particularly in the range $q = 2.0$ to 3.5 Å^{-1}. This is not surprising given that the OO radial distribution function of HDA is poorly reproduced by the ST2 model [41].

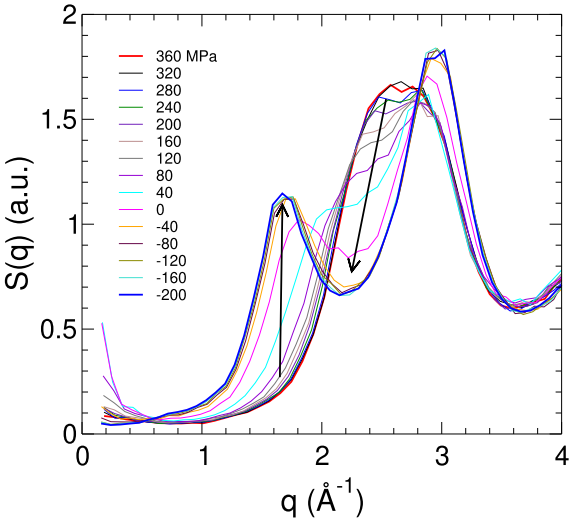

Fig. 5. Structure factor $S(q)$ for O atoms as a function of wave number q along the isothermal decompression at $T = 200$ K starting from HDA-d with initial density of 1.30 g/cm^3; see cyan curve in Fig. 4(a). $S(q)$ curves at various pressures are shown, from 360 MPa (HDA, thick red curve) to −200 MPa (LDA, thick blue curve). The arrows indicate the direction of *decreasing* pressure in our decompression simulations. As the system evolves from HDA/HDL to LDA/LDL, the contributions to S(q) in the range from $q = 2.0$ to 2.5 Å^{-1}, characteristic of HDA/HDL, decrease while the contributions from $q = 1.4$ to 2.0 Å^{-1}, characteristic of LDA/LDL, increase. (For interpretation of the references to color in this figure legend, the reader is referred to the web version of this article.)

Our results also show that regardless of whether the isothermal decompression process starts with HDA or HDL, the signature of the LLPT is observed, in the form of an inflection point in the variation with P of the order parameter ρ. As shown above, our results are also consistent with the interpretation of the evolution of the structure factor observed in Ref. [24] during the decompression stage of the experiment. Regardless of the initial state of the sample prior to decompression in our simulations, we note that at the decompression rate used here, none of the simulations that we conduct for $T < T_c$ access the equilibrium LDL state upon decompression; the low-density states in our simulations for $T < T_c$ are always LDA or non-equilibrium LDL. In the experiments of Ref. [24], the decompression rate is approximately 100 times slower, and in addition, crystallization does not begin until approximately 10 μs after the end of the IR heating stage. Ref. [24] shows that this time scale is sufficient to access equilibrium liquid LDL at the end of the decompression stage in the experiment (at $P \approx 0$).

5. Discussion

In summary, the results of our simulations as shown in Figs. 3 and 4 are consistent with the experiments of Ref. [24] and support the interpretation of the thermodynamic pathway presented there. We have shown that a process of rapid isochoric heating applied to HDA at $P = 0$ can be used to access the HDL phase at pressures above the coexistence line of the LLPT. Furthermore, when such a sample is decompressed isothermally, it will pass through the conditions of the LLPT and convert to the low-density phase, which is LDA or non-equilibrium LDL in our simulations and which is equilibrium LDL in the experiments. Furthermore, depending on the decompression temperature, the high-density to low-density transformation observed in our simulations can be smooth or sharp, but so long as $T < T_c$, the transition observed in our rapid decompression runs exhibits an inflection of the density as a function the pressure consistent with the discontinuous HDL-to-LDL transition of the equilibrium system. That is, despite the use of very fast heating and decompression rates, the influence of the underlying equilibrium behavior of the system remains observable during the strongly out-of-equilibrium process studied here.

We note that we do not expect finite-size effects to influence our

qualitative conclusions. Our results for $N = 1728$ molecules are consistent with results obtained in glassy ST2 water using $N = 1000$ [33]. Similarly, previous MD simulation studies of glassy water using the TIP4P/2005 water model show that the behavior of $\rho(P)$ during the compression-induced LDA-HDA transformations at $T < 200$ K is almost indistinguishable for $N = 512$ and $N = 8192$ [41,42].

Importantly, and as anticipated in Ref. [24], we find that due to the ultrafast decompression rate, neither the experimental nor the computational high-density to low-density transformation at $P_{H\to L}$ occurs at the equilibrium LDL-HDL coexistence pressure P_{coex}. Rather, as shown in Fig. 3, for $T < T_c$ we find that $P_{H\to L} < P_{coex}$. The position of the $P_{H\to L}$ curve depends on several factors, especially the decompression rate, and so it may vary widely between simulations and experiments. Nonetheless, Fig. 3 shows that the $P_{H\to L}$ curve observed in the ultrafast process studied here places a lower bound on the location of the equilibrium coexistence line of the LLPT. Notably, the $P_{H\to L}$ curve also converges to the location of the equilibrium LLCP in the P-T plane as $T \to T_c$. Fig. 3 further shows that the $P_{H\to L}$ curve overlaps with the HDL-to-LDL spinodal line evaluated from ST2 simulations of the equilibrium liquid in the range 235 K $< T < T_c$ [28]. As shown in SM Sec. I, we find that the range of T over which this overlap occurs increases when the decompression rate decreases. Our work thus demonstrates that if the pressure corresponding to the $P_{H\to L}$ curve as a function of T could be measured in an experiment, it would be possible to locate the equilibrium LLCP in real water using the ultrafast process pioneered in Ref. [24].

A broader conclusion may also be drawn by combining the present results with those reported in Refs. [33–38]. These studies collectively document the behavior of glassy ST2 water when subjected to a wide variety of heating, cooling, compression and decompression processes. As highlighted here, so long as the relevant rates q_T and q_P are constant, important boundaries defining the response of the system (e.g. T_g, $P_{H\to L}$, crystallization) can be predicted for one process (e.g. isochoric heating) using results found from another process (e.g. isothermal compression). That is, for practical purposes, one can define a phase diagram for glassy and supercooled ST2 water with well-defined boundaries between the LDA, HDA, LDL, and HDL when q_T and q_P are fixed. It would be interesting in future work to test if this result can be generalized to other water models. It would also be interesting to explore the implications of this finding for the definition of an out-of-equilibrium free energy function $F(N, V, T, q_T, q_P)$ for glassy water, and the corresponding phase diagram, that explicitly includes the rates as "state variables".

Supplemental material

In Sec. I of the SM, we test whether our results are sensitive to the compression/decompression rates employed. In Sec. II, we show how increasing the heating rate during isochoric heating affects the temperature dependence of the pressure and energy. Sec. III provides a brief description of dynamical and structural properties used to identify the HDA-to-HDL transformation and crystallization during the isochoric heating of HDA. In Sec. IV, we show that the results presented in the main manuscript are independent of the process followed to prepare the recovered HDA samples at $T = 80$ K and pressure P_i.

Data availability statement

The data that support the findings of this study are available from the corresponding authors upon reasonable request.

Declaration of Competing Interest

The authors declare that they have no known competing financial interests or personal relationships that could have appeared to influence the work reported in this paper.

Acknowledgments

PHP acknowledges the support of the Natural Sciences and Engineering Research Council of Canada (NSERC), Grant Number RGPIN-2017-04512. We also thank ACENET and Compute Canada for support. We thank K. Amann-Winkel, K. H. Kim, and A. Nilsson for valuable discussions. We thank F. Sciortino for providing the code to evaluate $S(q)$ as presented in Fig. 5. We dedicate this work to the memory of C. Austen Angell, a dear friend and remarkable experimentalist, who was also an innovator in the use of computer simulations to illuminate experimental results for water and many other systems.

Appendix A. Supplementary data

Supplementary data to this article can be found online at https://doi.org/10.1016/j.nocx.2021.100067.

References

[1] C.A. Angell, J. Shuppert, J.C. Tucker, Anomalous properties of supercooled water. Heat capacity, expansivity, and proton magnetic resonance chemical shift from 0 to −38 C, J. Phys. Chem. 77 (26) (1973) 3092–3099, https://doi.org/10.1021/j100644a014.
[2] R.J. Speedy, C.A. Angell, Isothermal compressibility of supercooled water and evidence for a thermodynamic singularity at −45 C, J. Chem. Phys. 65 (3) (1976) 851–858, https://doi.org/10.1063/1.433153.
[3] P.H. Poole, F. Sciortino, U. Essmann, H.E. Stanley, Phase behaviour of metastable water, Nature 360 (6402) (1992) 324–328, https://doi.org/10.1038/360324a0.
[4] J.A. Sellberg, C. Huang, T.A. McQueen, N.D. Loh, H. Laksmono, D. Schlesinger, R. G. Sierra, D. Nordlund, C.Y. Hampton, D. Starodub, D.P. DePonte, M. Beye, C. Chen, A.V. Martin, A. Barty, K.T. Wikfeldt, T.M. Weiss, C. Caronna, J. Feldkamp, L.B. Skinner, M.M. Seibert, M. Messerschmidt, G.J. Williams, S. Boutet, L.G. M. Pettersson, M.J. Bogan, A. Nilsson, Ultrafast X-ray probing of water structure below the homogeneous ice nucleation temperature, Nature 510 (7505) (2014) 381–384, https://doi.org/10.1038/nature13266.
[5] H. Pathak, A. Spah, N. Esmaeildoost, J.A. Sellberg, K.H. Kim, F. Perakis, K. Amann-Winkel, M. Ladd-Parada, J. Koliyadu, T.J. Lane, C. Yang, H.T. Lemke, A. R. Oggenfuss, P.J.M. Johnson, Y. Deng, S. Zerdane, R. Mankowsky, P. Beaud, A. Nilsson, Enhancement and maximum in the isobaric specific-heat capacity measurements of deeply supercooled water using ultrafast calorimetry, Proc. Natl. Acad. Sci. USA 118 (6) (2021), https://doi.org/10.1073/pnas.2018379118 e2018379118.
[6] L. Kringle, W.A. Thornley, B.D. Kay, G.A. Kimmel, Reversible structural transformations in supercooled liquid water from 135 to 245K, Science 369 (6510) (2020) 1490–1492, https://doi.org/10.1126/science.abb7542.
[7] L. Kringle, W.A. Thornley, B.D. Kay, G.A. Kimmel, Structural relaxation and crystallization in supercooled water from 170 to 260K, Proc. Natl. Acad. Sci. USA 118 (14) (2021), https://doi.org/10.1073/pnas.2022884118 e2022884118.
[8] V. Holten, C. Qiu, E. Guillerm, M. Wilke, J. Rička, M. Frenz, F. Caupin, Compressibility anomalies in stretched water and their interplay with density anomalies, J. Phys. Chem. Lett. 8 (22) (2017) 5519–5522, https://doi.org/10.1021/acs.jpclett.7b02563.
[9] K. Winkel, E. Mayer, T. Loerting, Equilibrated high-density amorphous ice and its first-order transition to the low-density form, J. Phys. Chem. B 115 (48) (2011) 14141–14148, https://doi.org/10.1021/jp203985w.
[10] Y. Suzuki, O. Mishima, Experimentally proven liquid–liquid critical point of dilute glycerol-water solution at 150K, J. Chem. Phys. 141 (9) (2014) 094505, https://doi.org/10.1063/1.4894416.
[11] O. Mishima, H.E. Stanley, The relationship between liquid, supercooled and glassy water, Nature 396 (6709) (1998) 329–335, https://doi.org/10.1038/24540.
[12] P.G. Debenedetti, H.E. Stanley, Supercooled and glassy water, Phys. Today 56 (6) (2003) 40–46, https://doi.org/10.1063/1.1595053.
[13] K. Amann-Winkel, R. Böhmer, F. Fujara, C. Gainaru, B. Geil, T. Loerting, Colloquium: water's controversial glass transitions, Rev. Mod. Phys. 88 (1) (2016) 011002, https://doi.org/10.1103/revmodphys.88.011002.
[14] C.A. Angell, Amorphous water, Ann. Rev. Phys. Chem. 55 (1) (2004) 559–583, https://doi.org/10.1146/annurev.physchem.55.091602.094156.
[15] A. Nilsson, L.G.M. Pettersson, The structural origin of anomalous properties of liquid water, Nat. Commun. 6 (1) (2015) 8998, https://doi.org/10.1038/ncomms9998.
[16] P. Gallo, K. Amann-Winkel, C.A. Angell, M.A. Anisimov, F. Caupin, C. Chakravarty, E. Lascaris, T. Loerting, A.Z. Panagiotopoulos, J. Russo, J.A. Sellberg, H.E. Stanley, H. Tanaka, C. Vega, L. Xu, L.G.M. Pettersson, Water: a tale of two liquids, Chem. Rev. 116 (13) (2016) 7463–7500, https://doi.org/10.1021/acs.chemrev.5b00750.
[17] P.G. Debenedetti, Supercooled and glassy water, J. Phys.: Condens. Matter 15 (45) (2003) R1669, https://doi.org/10.1088/0953-8984/15/45/r01.
[18] P.H. Handle, T. Loerting, F. Sciortino, Supercooled and glassy water: metastable liquid(s), amorphous solid(s), and a no-man's land, Proc. Natl. Acad. Sci. USA 114 (51) (2017) 13336–13344, https://doi.org/10.1073/pnas.1700103114.

[19] O. Mishima, H.E. Stanley, Decompression-induced melting of ice IV and the liquid–liquid transition in water, Nature 392 (6672) (1998) 164–168, https://doi.org/10.1038/32386.
[20] O. Mishima, Polyamorphism in water, Proc. Jpn. Acad. Ser. B 86 (3) (2010) 165–175, https://doi.org/10.2183/pjab.86.165.
[21] A. Späh, H. Pathak, K.H. Kim, F. Perakis, D. Mariedahl, K. Amann-Winkel, J. A. Sellberg, J.H. Lee, S. Kim, J. Park, K.H. Nam, T. Katayama, A. Nilsson, Apparent power-law behavior of water's isothermal compressibility and correlation length upon supercooling, Phys. Chem. Chem. Phys. 21 (1) (2018) 26–31, https://doi.org/10.1039/c8cp05862h.
[22] N.J. Hestand, J.L. Skinner, Perspective: crossing the widom line in no man's land: experiments, simulations, and the location of the liquid–liquid critical point in supercooled water, J. Chem. Phys. 149 (14) (2018) 140901, https://doi.org/10.1063/1.5046687.
[23] J.C. Palmer, P.H. Poole, F. Sciortino, P.G. Debenedetti, Advances in computational studies of the liquid–liquid transition in water and water-like models, Chem. Rev. 118 (18) (2018) 9129–9151, https://doi.org/10.1021/acs.chemrev.8b00228.
[24] K.H. Kim, K. Amann-Winkel, N. Giovambattista, A. Späh, F. Perakis, H. Pathak, M. L. Parada, C. Yang, D. Mariedahl, T. Eklund, T.J. Lane, S. You, S. Jeong, M. Weston, J.H. Lee, I. Eom, M. Kim, J. Park, S.H. Chun, P.H. Poole, A. Nilsson, Experimental observation of the liquid–liquid transition in bulk supercooled water under pressure, Science 370 (6519) (2020) 978–982, https://doi.org/10.1126/science.abb9385.
[25] J.C. Palmer, F. Martelli, Y. Liu, R. Car, A.Z. Panagiotopoulos, P.G. Debenedetti, Metastable liquid–liquid transition in a molecular model of water, Nature 510 (7505) (2014) 385–388, https://doi.org/10.1038/nature13405.
[26] F. Smallenburg, P.H. Poole, F. Sciortino, Phase diagram of the ST2 model of water, Mol. Phys. 113 (17–18) (2015) 2791–2798, https://doi.org/10.1080/00268976.2015.1043966.
[27] Y. Liu, A.Z. Panagiotopoulos, P.G. Debenedetti, Low-temperature fluid-phase behavior of ST2 water, J. Chem. Phys. 131 (10) (2009) 104508, https://doi.org/10.1063/1.3229892.
[28] P.H. Poole, I. Saika-Voivod, F. Sciortino, Density minimum and liquid–liquid phase transition, J. Phys.: Condens. Matter 17 (43) (2005) L431, https://doi.org/10.1088/0953-8984/17/43/l01.
[29] F.H. Stillinger, A. Rahman, Improved simulation of liquid water by molecular dynamics, J. Chem. Phys. 60 (4) (1974) 1545–1557, https://doi.org/10.1063/1.1681229.
[30] P.H. Poole, S.R. Becker, F. Sciortino, F.W. Starr, Dynamical behavior near a liquid–liquid phase transition in simulations of supercooled water, J. Phys. Chem. B 115 (48) (2011) 14176–14183, https://doi.org/10.1021/jp204889m.
[31] M.J. Cuthbertson, P.H. Poole, Mixturelike behavior near a liquid–liquid phase transition in simulations of supercooled water, Phys. Rev. Lett. 106 (2011) 115706, https://doi.org/10.1103/PhysRevLett.106.115706.
[32] P.H. Poole, U. Essmann, F. Sciortino, H.E. Stanley, Phase diagram for amorphous solid water, Phys. Rev. E 48 (6) (1993) 4605–4610, https://doi.org/10.1103/physreve.48.4605.
[33] N. Giovambattista, T. Loerting, B.R. Lukanov, F.W. Starr, Interplay of the glass transition and the liquid–liquid phase transition in water, Sci. Rep. 2 (1) (2012) 390, https://doi.org/10.1038/srep00390.
[34] J. Chiu, F.W. Starr, N. Giovambattista, Pressure-induced transformations in computer simulations of glassy water, J. Chem. Phys. 139 (18) (2013) 184504, https://doi.org/10.1063/1.4829276.
[35] J. Chiu, F.W. Starr, N. Giovambattista, Heating-induced glass-glass and glass-liquid transformations in computer simulations of water, J. Chem. Phys. 140 (11) (2014) 114504, https://doi.org/10.1063/1.4868028.
[36] N. Giovambattista, F. Sciortino, F.W. Starr, P.H. Poole, Potential energy landscape of the apparent first-order phase transition between low-density and high-density amorphous ice, J. Chem. Phys. 145 (22) (2016) 224501, https://doi.org/10.1063/1.4968047.
[37] N. Giovambattista, F.W. Starr, P.H. Poole, Influence of sample preparation on the transformation of low-density to high-density amorphous ice: an explanation based on the potential energy landscape, J. Chem. Phys. 147 (4) (2017) 044501, https://doi.org/10.1063/1.4993567.
[38] N. Giovambattista, F.W. Starr, P.H. Poole, State variables for glasses: the case of amorphous ice, J. Chem. Phys. 150 (22) (2019) 224502, https://doi.org/10.1063/1.5092586.
[39] M.P. Allen, D.J. Tildesley, Computer Simulation of Liquids, Second Edition, Oxford University Press, 2017, https://doi.org/10.1093/oso/9780198803195.001.0001.
[40] T. Loerting, N. Giovambattista, Amorphous ices: experiments and numerical simulations, J. Phys.: Condens. Matter 18 (50) (2006) R919, https://doi.org/10.1088/0953-8984/18/50/r01.
[41] J. Wong, D.A. Jahn, N. Giovambattista, Pressure-induced transformations in glassy water: a computer simulation study using the TIP4P/2005 model, J. Chem. Phys. 143 (7) (2015) 074501, https://doi.org/10.1063/1.4928435.
[42] J. Engstler, N. Giovambattista, Heating- and pressure-induced transformations in amorphous and hexagonal ice: a computer simulation study using the TIP4P/2005 model, J. Chem. Phys. 147 (7) (2017) 074505, https://doi.org/10.1063/1.4998747.

June 22, 2021

Supplemental Material: Liquid-liquid phase transition in simulations of ultrafast heating and decompression of amorphous ice

Nicolas Giovambattista[*,1,2] and Peter H. Poole[*,3]

[1] *Department of Physics, Brooklyn College of the City University of New York, Brooklyn, NY 11210, United States*

[2] *Ph.D. Programs in Chemistry and Physics, The Graduate Center of the City University of New York, New York, NY 10016, United States*

[3] *Department of Physics, St. Francis Xavier University, Antigonish, Nova Scotia B2G 2W5, Canada*

[*] *Electronic mail: ngiovambattista@brooklyn.cuny.edu, ppoole@stfx.ca*

I. SIMULATIONS USING A SLOWER COMPRESSION/DECOMPRESSION RATE

In the main manuscript, the HDA forms recovered at $T = 80$ K and pressure P_i, which are used as starting configurations in the isobaric heating runs, correspond to HDA-d. In particular, all compression/decompression runs are performed at the rate $q_P = 300$ MPa/ns. In this section, we repeat the heating-decompression simulations described in the main manuscript but using a slower compression/decompression rate of $q_P = 30$ MPa/ns, closer to the estimated experimental rate.

First we obtain new samples of HDA-d by compression of LDA at $T = 80$ K and $q_P = 30$ MPa/ns from $P = 0.1$ MPa to $P = 1500$ MPa. The resulting HDA is then decompressed at $T = 80$ K to $P_i \approx 0$, yielding HDA-d. For simplicity, we only consider the case where of starting HDA-d samples have a density $\rho_i = 1.36$ g/cm^3 at $T = 80$ K, giving P_i in the range from 0 to 150 MPa.

These new HDA-d samples are then heated isochorically at the same rate used in the main manuscript, i.e., $q_T = 30$ K/ns. Fig. S1 shows the trajectories of our ten independent runs upon heating HDA-d at constant $\rho_i = 1.36$ g/cm^3. Fig. S1 is analogous to Fig. 3 of the main manuscript, and the results in these two figures are qualitatively identical. For the HDA-d samples prepared at $q_P = 30$ MPa/ns, we find that nine of the ten independent runs crystallize upon heating. In Fig. S1, we show the single trajectory that extends into the liquid state without signs of crystallization. For comparison, also included is one of the trajectories that exhibit crystallization. The remaining trajectories are shown up to the temperature where crystallization occurs ($T \leq 240$ K).

The same boundary lines shown in Fig. 3 of the main manuscript (for $q_P = 300$ MPa) are included in Fig. S1: (i) The black solid line indicates the crystallization (nose-shaped) region at high pressures determined during isothermal compression in Ref. [1]. (ii) The orange up-triangles at $T = 250$ K indicate the temperature at which HDA/HDL crystallize during isobaric heating at $P > 400$ MPa ($q_T = 30$ K/ns). (iii) The maroon dashed-line represents the P-T conditions at which the HDA-to-LDA and HDA-to-HDL transformations occur upon isobaric heating [2] with $q_T = 30$ K/ns. (iv) The solid orange left-triangles indicate the HDA/HDL-to-LDA/LDL transformation reported during isothermal decompression in Ref. [1]. (v) The solid indigo left-triangles indicate the pressures at which the recovered LDA

forms fracture upon isothermal decompression. The boundary lines (i)-(v) are valid when all the compression/decompression runs are performed with rate $q_P = 300$ MPa/ns. Reducing the rate to $q_P = 30$ MPa/ns does not affect (v); see indigo empty left-triangles. However, it increases the size of the crystallization region (i) at high pressures; the crystallization region obtained using $q_P = 30$ MPa/ns is indicated by the black empty right-triangles. Similarly, reducing q_P shifts the boundary (iv) towards higher pressures; the HDA/HDL-to-LDA/LDL transformation line obtained during isothermal decompression at $q_P = 30$ MPa/ns is indicated by empty orange left-triangles (see Ref. [1]). One of the main points of Fig. S1 is that the temperature at which HDA-d reaches the liquid state, $P \approx 550$ MPa and $T \approx 210-220$ K (see Sec. III), occurs at the intersection of the magenta lines with the maroon dashed-line, i.e., at the glass transition temperature of HDA determined independently from isobaric heating runs at the same heating rate $q_T = 30$ K/ns employed here; see Ref. [2].

The HDA/HDL samples obtained by isochoric heating to the temperature $T = T_f$ are then subjected to isothermal decompression at this T. Fig. S2 shows the density as function of temperature for HDA/HDL samples decompressed at different $T \leq 210$ K. (At $T > 210$ K crystallization occurs either during the heating runs or upon isothermal decompression). As reported in Fig. 4 of the main manuscript, we find that the HDA/HDL-to-LDA/LDL transformation is rather sharp at all $T \leq 210$ K. The HDA/HDL-to-LDA/LDL transformation pressures $P_{\mathrm{H}\to\mathrm{L}}$ are included in Fig. S1 (magenta left-triangles). In agreement with the discussion in the main manuscript, $P_{\mathrm{H}\to\mathrm{L}}$ (magenta left-triangles) overlaps with the HDA/HDL-to-LDA/LDL transformation pressures (empty orange left-triangles) obtained in Ref. [1] upon isothermal decompression of HDA/HDL at $q_P = 30$ MPa/ns. That is, reducing q_P shifts the decompression-induced HDA/HDL-to-LDA/LDL transformation towards higher pressures. Nonetheless, the $P_{\mathrm{H}\to\mathrm{L}}$ line determined during ultrafast heating-decompression simulations still coincides with the HDA/HDL-to-LDA/LDL transformation pressures determined during isothermal compression-decompression cycles of LDA to HDA and back, when conducted at the same rate q_P.

II. INCREASING THE RATE OF ISOCHORIC HEATING

Here we test the effect of increasing the rate of heating q_T used in our isochoric heating runs that start with HDA-d at $T = 80$ K and $\rho_i = 1.30$ g/cm^3. Fig. S3 shows P and E as a

function of T using $q_T = 30$, 300 and 3000 K/ns. We find that as q_T increases, the variation of P with T at fixed density becomes more linear, the result that would be expected when the ideal gas contribution to the pressure dominates. Despite the very fast heating rates explored here, all our runs give similar values for P and E when the system accesses the liquid state for $T > T_g \approx 220$ K.

III. GLASS TRANSITION AND CRYSTALLIZATION UPON ISOCHORIC HEATING

Next, we discuss briefly the glass transition of HDA-d and crystallization reported during isochoric heatings. For simplicity, we focus on the heating runs discussed in Sec. I above. The phenomenology is reminiscent to the HDA-to-ice, HDA-to-HDL, and HDA-to-HDL-to-ice transformations reported in Ref. [2] upon *isobaric* heating.

Fig. S4 shows the pressure P and total energy E as function of temperature upon heating HDA-d at $\rho_i = 1.36$ g/cm^3. Crystallization is observed in most of the independent runs (red lines). Only one trajectory shows no signs of crystallization (black line). The corresponding mean-square displacement (MSD) of the water O atoms as function of temperature is shown in Fig. S5.

At the employed heating rate, $q_T = 30$ K/ns, the MSD is negligible up to $T \approx 220$ K and then starts to increase rapidly upon further heating. At $T = 250$ K, the MSD reaches approximately 0.6 to 0.8 nm^2, suggesting that molecules have displaced by approximately 0.8 to 0.9 nm, i.e., > 2 times the separation between OO nearest-neighbors. It follows that all samples remain in the HDA-d state until the glass transition temperature $T_g \approx 220$ K is reached at $P \approx 550$ MPa. Again, this temperature is very close to the glass transition temperature of HDA obtained upon *isobaric* heating of HDA at $P \approx 550$ MPa and $T \approx 225$ K with $q_T = 30$ K/ns. Consistent with the behavior of the MSD, the total energy increases almost linearly with increasing T for $T < 220$ K, while the samples are in the HDA-d state. As shown in Fig. S4a, all samples reach the same P at $T \approx 200$ K, slightly below T_g.

Upon further heating at $T > 220$ K, the samples show different behaviors. When crystallization is avoided (black line), the MSD and E both increase monotonically with T upon heating, as expected for a system in the liquid state. Indeed, as shown in Fig. S6a, the OO radial distribution function (RDF) of the system at different temperatures shows no indica-

tion of crystallization. Specifically, the RDF reaches the value ≈ 1 at $r \approx 1$ nm indicating that there is only short range order in the sample.

In the case where crystallization occurs (red lines), the MSD, E and P decrease sharply with T at the crystallization temperature T_x. Not surprisingly, crystallization among the different runs occurs randomly in the range $T_x = 240$ to 260 K. Crystallization is confirmed by the RDF of the system; see Fig. S6b. We note that the RDF of the system at $T = 260$ K is indeed similar to that reported in Ref. [2] for ice VII which was found to form during isobaric heating of HDA-d at $P > 400$ MPa with $q_T = 30$ K/ns. It follows from our discussion that, at the present ultrafast rates, the samples must reach a HDL-like state over the short temperature interval ($T_g = 220$ K) $< T <$ ($T_x = 240$ to 260 K). Indeed, a similar sequence of transformations from HDA-d to HDL to ice VII upon isobaric heating was reported in Ref. [2].

Upon further heating, the ultra-fast heating rate employed in this work forces the crystal to at least partially melt. Specifically, the MSD, E and P increase sharply with T at $T > 300$ K, consistent with a fraction of the system returning to the liquid state. Fig. S6b shows that the structure of the samples retains features of the crystal RDF up to 340 K, suggesting that melting is not complete in these runs. Since our heating runs are carried out at constant volume, the system may be in a state of liquid-ice coexistence.

IV. ROLE OF THE PROCESS FOLLOWED TO PREPARE RECOVERED HDA

Glasses, in general, and amorphous ices, in particular, are history-dependent materials. Accordingly, the process followed in the preparation of the starting HDA sample could affect the outcome of ultrafast heating-decompression experiments or computer simulations [3, 4]. In this section, we show that our results as presented in the main manuscript are robust relative to the method of preparing the starting HDA sample at $T = 80$ K and ρ_i.

In the main manuscript, the starting HDA sample for the heating runs is HDA-d. In this section, we use a different HDA form, termed "HDA-i", which was studied in detail in Refs. [1–5]. Briefly, HDA-i samples are prepared from HDL configurations equilibrated at $P = 400$ MPa and at temperatures $T_0 \geq T_g$. Here we choose $T_0 = 220$ and 300 K. After equilibration at T_0, the HDL samples are cooled instantaneously to $T = 80$ K by rescaling the velocities of all atoms in the system, producing HDA. That is, these HDA-i

samples are obtained using an infinite cooling rate. It follows that the so produced HDA-i samples have the same density and are structurally identical to the equilibrium HDL at the starting temperature T_0 and $P = 400$ MPa. We note that the HDA-i forms obtained from different temperatures T_0 can exhibit slightly different structural and thermodynamic properties [3, 4]. We stress that, since HDA-i is obtained from the equilibrium HDL, our HDA-i samples are completely unrelated to our HDA-d samples.

The HDA-i samples produced at $P = 400$ MPa and $T = 80$ K are then isothermally compressed/decompressed at rate $q_P = 300$ MPa/ns at $T = 80$ K until they reach the density $\rho_i = 1.30$ g/cm^3. In the case of $T_0 = 220$ K [$T_0 = 300$ K], the pressure of the resulting HDA-i samples are within the interval $(200, 400)$ MPa [$(525, 800)$ MPa]. These HDA-i samples at $\rho_i = 1.30$ g/cm^3 and $T = 80$ K are used as starting configurations for the heating runs described in the step (i) of Fig. 1 in the main manuscript.

Fig. S7 shows the trajectory in the P-T plane of the HDA-i samples heated at constant $\rho_i = 1.30$ g/cm^3. For comparison, we also include the trajectories followed by HDA-d samples heated at the same density ρ_i, taken from Fig. 1 (green lines) of the main manuscript. The pressures of the HDA-i samples at the initial temperature $T = 80$ K are indeed very different: $P_i = 200$ to 400 MPa for the HDA-i prepared from the liquid at $T_0 = 220$ K (red lines), and $P_i = 550$ to 800 MPa when $T_0 = 300$ K (dark green lines). These pressures are considerably larger than the pressures of HDA-d, which have $-100 \leq P \leq -50$ MPa. It follows that, upon heating, HDA-d, HDA-i ($T_0 = 220$ K), and HDA-i ($T_0 = 300$ K) all follow different paths within the glass domain. In this glass regime, in the range $T < 200$ K, the pressure of all the HDA samples varies non-linearly with increasing temperature when $q_T = 30$ K/ns.

At $T \approx 200$ K, all HDA forms studied reach the same pressure of $P \approx 400$ MPa. This is because all these HDA forms have the same density ρ_i and reach the glass transition at $T \approx 210$ K and $P = 400$ MPa when $q_T = 30$ K/ns. Accordingly, HDA-d and HDA-i must transforms to the same equilibrium liquid state at $T \approx 210$ K and $P \approx 400$ MPa. This also explains why all heating runs follow a common path in the P-T plane when $T > 210$ K. In this liquid regime, we find that approximately $P \propto T$.

Despite the different behavior of HDA-d and HDA-i in the glass state, the behavior of HDA-d, HDA-i ($T_0 = 220$ K), and HDA-i ($T_0 = 300$ K) during isothermal decompression is very similar; see Fig. S8. This similarity is to be expected for samples decompressed at $T > T_g$ for HDA, since these samples all begin the decompression process from the

equilibrium HDL phase. However, the similarity also applies to the decompression runs conducted at $T < T_g$, in which case the HDA-d and HDA-i samples are distinct glasses, with distinct preparation histories. In particular, we find only very small differences in the transformation pressure $P_{\mathrm{H}\to\mathrm{L}}$. The $P_{\mathrm{H}\to\mathrm{L}}$ lines for HDA-d, HDA-i ($T_0 = 220$ K), and HDA-i ($T_0 = 300$ K) are indicated in Fig. S7 by green, red, and dark-green empty left-triangles, respectively. Fig. S7 therefore supports the robustness of the results reported during the ultrafast heating-decompression pathway considered here, both from computer simulations and experiments.

[1] J. Chiu, F. W. Starr, and N Giovambattista, J. Chem. Phys. **139**, 184504 (2013).

[2] J. Chiu, F. W. Starr, and N Giovambattista, J. Chem. Phys. **140**, 114504 (2013).

[3] N. Giovambattista, F. W. Starr, and P. H. Poole, J. Chem. Phys. **147**, 044501 (2017).

[4] N. Giovambattista, F. W. Starr, and P. H. Poole, J. Chem. Phys. **150**, 224502 (2019).

[5] N. Giovambattista, F. Sciortino, F. W. Starr, and P. H. Poole, J. Chem. Phys. **145**, 224501 (2016).

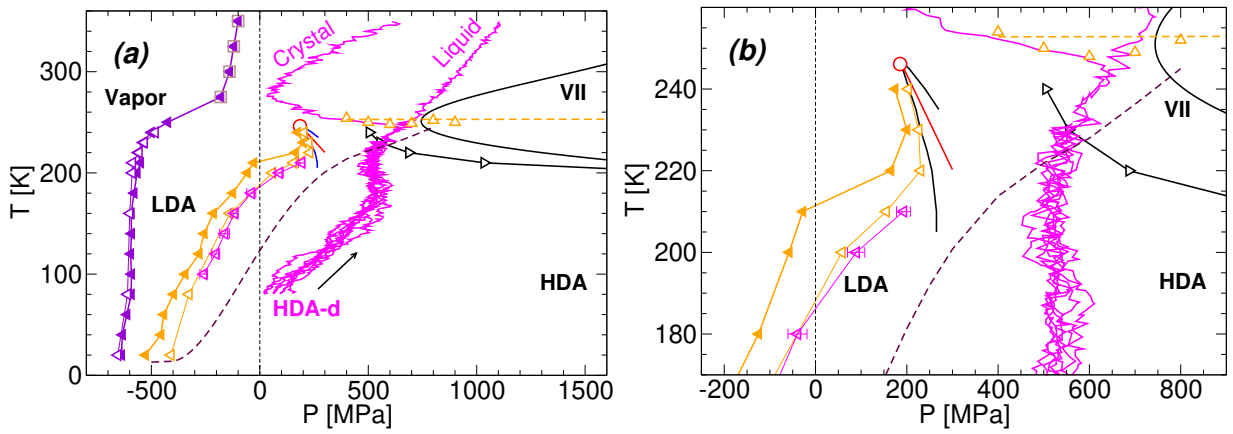

FIG. S1: Same as Fig. 3 of the main manuscript for the case of HDA-d samples obtained using a slower compression/decompression rate $q_P = 30$ MPa/ns. Temperature as function of pressure upon heating HDA-d at $\rho_i = 1.36$ g/cm^3 (magenta lines) with $q_T = 30$ K/ns. The starting HDA-d configurations are obtained by decompressing HDA at $T = 80$ K from $P = 1500$ MPa until the system reaches the target density ρ_i; see green lines in Fig. 2b of the main manuscript for the case $q_P = 30$ MPa/ns. Empty magenta left-triangles represent the HDA/HDL-to-LDA/LDA transformation obtained upon isothermal decompression of samples formed during heating of HDA-d at ρ_i; see also Fig. S2. Solid violet and orange left-triangles represent, respectively, the pressure at which LDA fractures and the HDA-to-LDA transformation upon decompression at the fast rate $q_P = 300$ MPa from Fig. 3 of the main manuscript. The corresponding transformation lines obtained at $q_P = 30$ MPa/ns are indicated by empty violet and orange left-triangles [1, 2]. Squares are the equilibrium liquid-to-vapor spinodal line. The maroon dashed line indicates the transformation of HDA to LDA (at low pressure) and HDA to HDL (at high pressure) upon isobaric heating. The orange up-triangles signal the temperature at which HDA crystallizes upon isobaric heating [2].

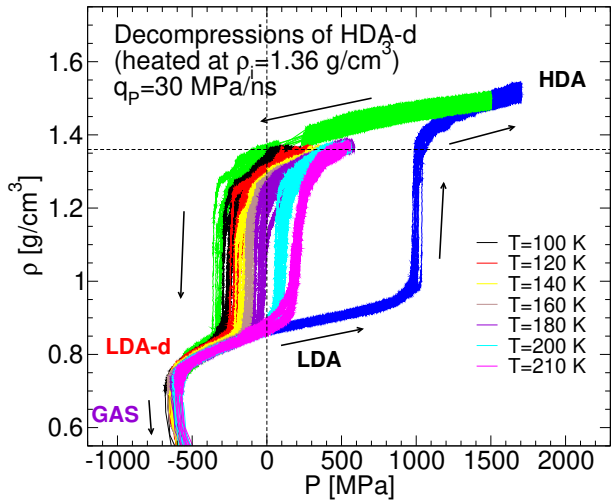

FIG. S2: Same as Fig. 4b of the main manuscript for the HDA-d samples obtained with the slower compression/decompression rate $q_P = 30$ MPa/ns. The starting HDA/HDL samples for the decompression runs at temperature T are prepared by isochoric heating of HDA-d at density $\rho_i = 1.36$ g/cm^3, from $T = 80$ K to the target temperature T. Blue and green lines are the pressure-induced LDA-to-HDA and HDA-to-LDA transformations at $T = 80$ K at the slower rate $q_P = 30$ MPa/ns, as also shown in Fig. 2b of the main manuscript. HDA-d samples crystallize during heating or decompression at $T > 210$ K.

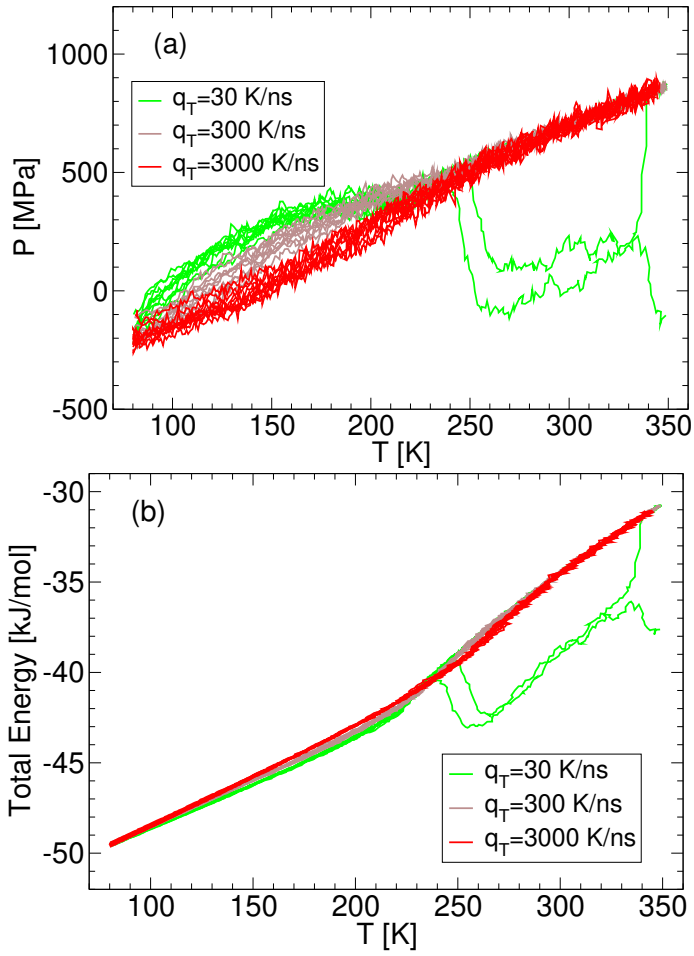

FIG. S3: (a) Pressure and (b) total energy as function of temperature during the isochoric heating of HDA-d at $\rho_i = 1.30$ g/cm^3 at different heating rates q_T. Two runs out of 10 for $q_T = 30$ K/ns (green lines) show crystallization. All other runs remain in the glass or liquid state.

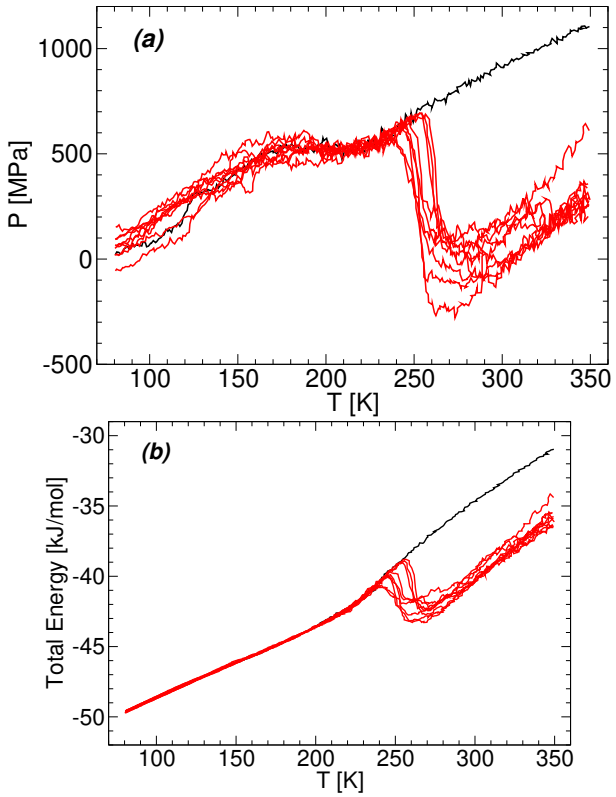

FIG. S4: (a) Pressure and (b) total energy as function of temperature during the isochoric heating of HDA-d at $\rho_i = 1.36$ g/cm^3 with $q_T = 30$ K/ns (see also magenta lines in Fig. S1). The starting HDA-d was produced from LDA with a compression/decompression rate $q_P = 30$ MPa/ns at $T = 80$ K. From the ten independent runs, only one trajectory does not show crystallization (black line); the rest crystallize at approximately $T > 230$ K (red lines). At low temperatures the system is in the HDA-d state and, at the present heating rate, it enters the liquid state at $T \approx 220$ K. Crystallization occurs randomly at $T_x = 240 - 260$ K (red lines) and some trajectories briefly reach the liquid state before crystallization occurs.

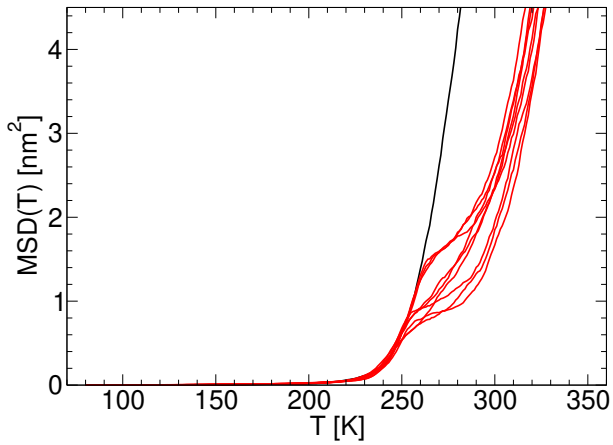

FIG. S5: Mean-square displacement (MSD) of O atoms as function of temperature during the isochoric heating of HDA-d at $\rho_i = 1.36$ g/cm^3 with $q_T = 30$ K/ns; see also Fig. S4. The MSD is calculated relative to the starting configuration of the system at $T = 80$ K. Molecules do not displace significantly until $T \approx 220$ K and so the system remains in the HDA-d state at these temperatures. At $T \approx 220$ K, the molecules start to diffuse and the MSD increases rapidly indicating that the system reaches a liquid-like state. Nine out of ten independent runs crystallize at temperatures in the range $T = 240$ to 260 K (red lines). The fast heating rate causes the crystal to subsequently melt.

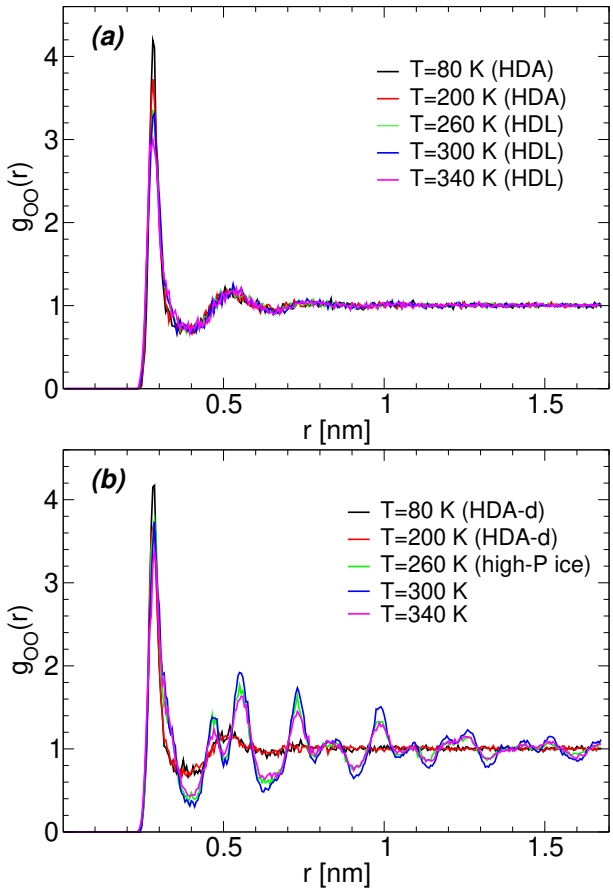

FIG. S6: Oxygen-Oxygen RDFs at selected temperatures upon heating HDA-d at $\rho_i = 1.36$ g/cm^3; see also Fig. S4. (a) RDF of the single sample that does not crystallize upon heating (black line in Fig. S4). (b) RDF of one of the samples that crystallizes upon heating.

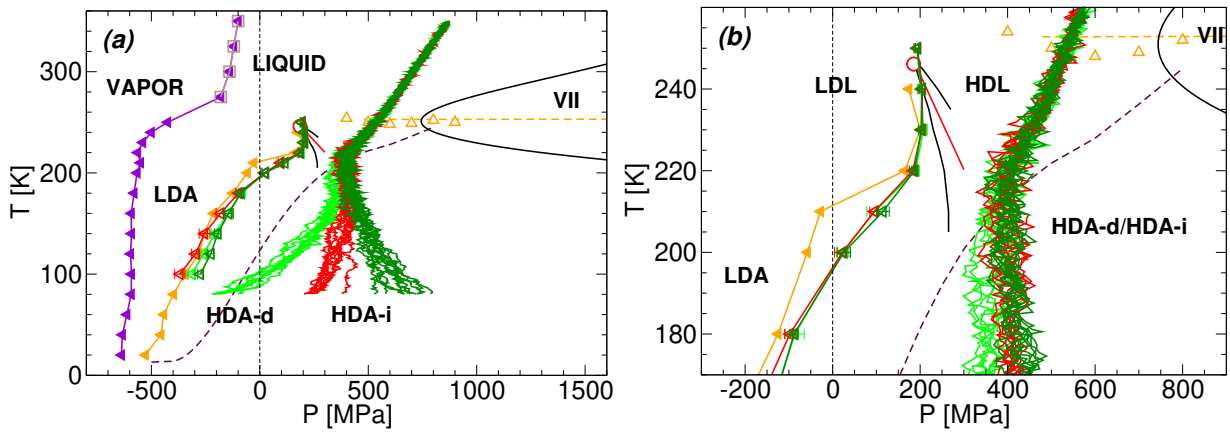

FIG. S7: Same as Fig. 3 of the main manuscript but for the case of HDA-i. Temperature as function of pressure upon heating HDA-i at $\rho_i = 1.30$ g/cm^3 (red and dark green lines). Red (dark green) lines correspond to HDA-i obtained by cooling instantly ($q_T = \infty$) the equilibrium liquid from $T_0 = 220$ K ($T_0 = 300$ K) to $T = 80$ K at constant $P = 400$ MPa. Empty dark-green and red left-triangles represent the (HDA-i)-to-LDA transformation obtained upon isothermal decompression of HDA-i samples at different tempeartures T (dark-green triangles, for the case $T_0 = 300$ K, and red triangles, for $T_0 = 220$ K); see also Fig. S8. For comparison, we also include the density upon heating HDA-d at constant $\rho_i = 1.30$ g/cm^3 [(taken from Fig. 2 of the main manuscript (green lines)] and the corresponding (HDA-d)-to-LDA transformation pressure (empty green left-triangles). At $T \geq 180$ K, the transformation pressures to LDA/LDL are independent of whether one starts from HDA-i or HDA-d forms, i.e., the process followed to prepare HDA is not relevant. Minor differences in the (HDA-i)-to-LDA and (HDA-d)-to-LDA transformation pressures are present at $T < 180$ K.

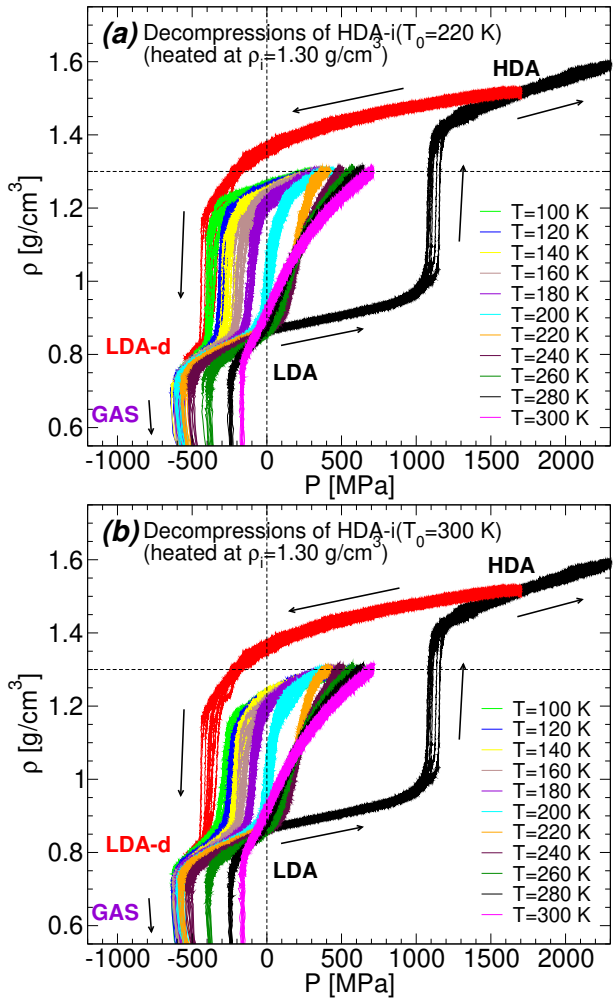

FIG. S8: Density as a function of pressure during the isothermal decompression of HDA-i samples heated to different temperatures T. The HDA-i samples are prepared by, first, cooling instantly ($q_T = \infty$) the liquid equilibrated at $P = 400$ MPa and (a) $T_0 = 220$ K and (b) $T = 300$ K to $T = 80$ K. The HDA-i forms are then decompressed/compressed ($T = 80$ K) until the density $\rho_i = 1.30$ g/cm^3 is reached. Samples are then heated at constant $\rho_i = 1.30$ g/cm^3, from $T = 80$ K to the target temperature T with heating rate $q_T = 30$ K/ns. Also included are the pressure-induced LDA-to-HDA and HDA-to-LDA transformations at $T = 80$ K from Fig. 2b of the main manuscript (black and red lines). All compression/decompression runs are performed at $q_P = 300$ MPa/ns. No crystallization occurs during decompression of HDA-i ($T_0 = 300$ K), while one of the ten decompression runs of HDA-i ($T_0 = 220$ K) exhibits crystallization at $T = 240, 250, 260, 260$ K. Similarly, two runs starting from HDA-d exhibit crystallization during decompression at $230 \leq T \leq 250$ K. Decompression trajectories that crystallize are omitted.